Journal of Hydrology 556 (2018) 585–599

Contents lists available at ScienceDirect

Journal of Hydrology

journal homepage: www.elsevier.com/locate/jhydrol

Research papers

Identification of dominant interactions between climatic seasonality, catchment characteristics and agricultural activities on Budyko-type equation parameter estimation

Wanqiu Xing [a,b], Weiguang Wang [a,c,*], Quanxi Shao [d], Bin Yong [a,b]

[a] State Key Laboratory of Hydrology-Water Resources and Hydraulic Engineering, Hohai University, Nanjing 210098, China
[b] School of Earth Sciences and Engineering, Hohai University, Nanjing 211100, China
[c] College of Water Resources and Hydrology, Hohai University, Nanjing 210098, China
[d] CSIRO Data 61, Private Bag 5, Wembley, Western Australia 6913, Australia

ARTICLE INFO

Article history:
Received 3 June 2017
Received in revised form 16 October 2017
Accepted 27 November 2017
Available online 2 December 2017
This manuscript was handled by G. Syme, Editor-in-Chief, with the assistance of Saeid Eslamian, Associate Editor

Keywords:
Budyko framework
Climate seasonality
Catchment characteristics
Agricultural activities
Multivariate adaptive regression splines
China

ABSTRACT

Quantifying precipitation (P) partition into evapotranspiration (E) and runoff (Q) is of great importance for global and regional water availability assessment. Budyko framework serves as a powerful tool to make simple and transparent estimation for the partition, using a single parameter, to characterize the shape of the Budyko curve for a "specific basin", where the single parameter reflects the overall effect by not only climatic seasonality, catchment characteristics (e.g., soil, topography and vegetation) but also agricultural activities (e.g., cultivation and irrigation). At the regional scale, these influencing factors are interconnected, and the interactions between them can also affect the single parameter of Budyko-type equations' estimating. Here we employ the multivariate adaptive regression splines (MARS) model to estimate the Budyko curve shape parameter (n in the Choudhury's equation, one form of the Budyko framework) of the selected 96 catchments across China using a data set of long-term averages for climatic seasonality, catchment characteristics and agricultural activities. Results show average storm depth (ASD), vegetation coverage (M), and seasonality index of precipitation (SI) are three statistically significant factors affecting the Budyko parameter. More importantly, four pairs of interactions are recognized by the MARS model as: The interaction between CA (percentage of cultivated land area to total catchment area) and ASD shows that the cultivation can weaken the reducing effect of high ASD (>46.78 mm) on the Budyko parameter estimating. Drought (represented by the value of Palmer drought severity index < -0.74) and uneven distribution of annual rainfall (represented by the value of coefficient of variation of precipitation > 0.23) tend to enhance the Budyko parameter reduction by large SI (>0.797). Low vegetation coverage (34.56%) is likely to intensify the rising effect on evapotranspiration ratio by IA (percentage of irrigation area to total catchment area). The Budyko n values estimated by the MARS model reproduce the calculated ones by the observation well for the selected 96 catchments (with R = 0.817, MAE = 4.09). Compared to the multiple stepwise regression model estimating the parameter n taken the influencing factors as independent inputs, the MARS model enhances the capability of the Budyko framework for assessing water availability at regional scale using readily available data.

1. Introduction

Quantifying the impacts of hydroclimatic changes on water availability is critical for regional water resource management and planning. On the catchment scale, water availability is substantially determined by the partitioning of precipitation (P) into evapotranspiration (E) and runoff (Q). However, dominated by numerous factors chiefly consisting of natural (e.g., climatic seasonality, topography) and anthropogenic factors (e.g., agricultural development), it is difficult to identify the partitioning process of P (Berghuijs et al., 2014; Greve et al., 2015). There are two categories of approaches to assess the water partitioning under changing environments: approaches based on detailed hydrologic models and simple conceptual model based on the Budyko hypothesis (Guo et al., 2015). With deterministic physical mechanisms, approaches based on detailed hydrologic models can accurately describe the hydrological processes yet the reliability of the

* Corresponding author at: State Key Laboratory of Hydrology-Water Resources and Hydraulic Engineering, Hohai University, Nanjing 210098, China.
E-mail addresses: wangweiguang2016@126.com, wangweiguang006@126.com (W. Wang).

https://doi.org/10.1016/j.jhydrol.2017.11.048
0022-1694/

simulation is always limited due to the model structures and parameter uncertainties. In practice, determining the impacts of climate change on board-scale water availability require long-term estimation (Teng et al., 2012; Singh and Kumar, 2015). Budyko framework, prescribing the dependence of long-term mean annual actual E on water supply (P) and demand (potential evaporation, E_0), serves as a simple but effective tool to make transparent estimates of changes in water availability, as well as to investigate the interactions between climate forcing and land surface characteristics on water and energy cycles (Roderick and Farquhar, 2011; Williams et al., 2012; Li et al., 2013; Berghuijs et al., 2014; Zhou et al., 2015; Greve et al., 2015; Fang et al., 2016; Wang et al., 2016).

The original Budyko hypothesis (Budyko, 1974) is that natural watersheds follow the Budyko curve, which is entirely deterministic and non-parametric. In this context, some non-parametric Budyko equations (e.g., Schreiber, 1904; Ol'dekop, 1911; Budyko, 1958; Pike, 1964) were developed. However, it should be acknowledged that variations around the curve can alter depending on land surface characteristics. Furthermore, many subsequently derived formulations of the Budyko curve are parametric (e.g., Mezentsev, 1955; Fu, 1981; Choudhury, 1999; Zhang et al., 2001; Porporato et al., 2004; Wang and Tang, 2014). Compared with non-parametric Budyko equations, single-parameter Budyko-type equations are more flexible to adapt to complicated watershed characteristics (Xiong and Guo, 2012). Playing the similar roles in controlling how much of the available water will be evaporated given the available energy, the empirical dimensionless parameters of different Budyko-type equations determine the shape of the Budyko curve and reflect the influences of basin characteristics (Xu et al., 2013). Consequently, a simple estimating model with precise characterization of the empirical dimensionless parameters will be a good basis for the Budyko framework application and water availability assessment.

Previous studies have documented that single-parameter in Budyko-type equations can be reflected by various climate and catchment characteristics, such as climatic seasonality characteristics (Milly, 1994; Potter et al., 2005; Williams et al., 2012; Chen et al., 2013; Berghuijs et al., 2014), soil properties (Porporato et al., 2004; Donohue et al., 2012), vegetation (Zhang et al., 2001; Donohue et al., 2007; Yang et al., 2009; Gentine et al., 2012; Li et al., 2013; Wang and Tang, 2014), groundwater (Istanbulluoglu et al., 2012), topographic controls (Shao et al., 2012; Xu et al., 2013), and relative area of ecological restoration (Liang et al., 2015). Moreover, numerous models (e.g., multiple stepwise regression, neural network techniques) have been proposed to estimate the parameters of Budyko-type equations for specific conditions (e.g., Yang et al., 2007, 2009; Donohue et al., 2012; Shao et al., 2012; Li et al., 2013; Xu et al., 2013). Unfortunately, those models are only based on climatic and catchment characteristics, the impact of changing anthropogenic factors on the partitioning of P into E and Q (reflecting by the single parameter in Budyko-type equation) has not been concerned in previous studies.

In fact, with the developing of global modernization, human activities (e.g. cultivation, irrigation, afforestation, deforestation and urban construction) have already altered land use/cover and evapotranspiration capacity. These activities further have been revealed to have increased or enhanced impacts on instream flow changes in recent years by extensive literatures (e.g., Brown et al., 2005; Scanlon et al., 2007; Roderick and Farquhar, 2011; Liu et al., 2017). Currently, Budyko hypothesis is usually used to quantify the impact of climate and humans on mean annual streamflow by the decomposition method or elasticity method (e.g., Wang and Hejazi, 2011; Chen et al., 2013; Tan and Gan, 2015; Liang et al., 2015; Jiang et al., 2015). For example, Wang and Hejazi (2011) used a decomposition method based on the Budyko hypothesis to quantify the climate and direct human impact on mean annual streamflow (MAS) for 413 watersheds in the contiguous United States, they found that direct human impact decreased mean annual streamflow in some watersheds with urban areas and extensively irrigated agriculture.

Globally, the irrigation area occupies 20% of the arable land area and sustains about 40% of the food production. Furthermore, the irrigation water diversion and consumption takes up respectively about 70% and 90% of the total human water diversion and consumption (Döll and Siebert, 2002; Wisser et al., 2008). The wide range activities of water diversion from rivers, reservoirs and underground aquifers to the irrigation districts significantly influenced the natural hydrological cycle. In some areas, the impact of irrigation is on the same order of magnitude as the impact of climate change. This is especially true in China, a vast agricultural country in the world. According to the statistics, the cultivated land accounts for about 12.5% of China's total land, and the irrigated land accounts for about 40% of China's total arable land and produces 75% of China's total food grain (Jin and Young, 2001). Thus, agricultural activities, especially cultivation and irrigation, which not only are vital for global food security, but also constitute land use changes, known to have strong effects on local hydrological and energy cycles (de Vrese et al., 2016). Hence, the hydrologic impact of changes in agricultural activities as well as changes in climatic seasonality characteristics and catchment characteristics should be also incorporated into the framework by changing the value of Budyko-type equations parameters. Besides, from the perspective of modelling precision, inclusion of more influencing factors can eliminate the problem of biased sampling and reduce model uncertainty (Shao et al., 2012). Therefore, in this work, we will highlight changes in those agricultural activities to emphasize the point that changes in the "specific basin" parameter may be subtle, not linearity related to the climatic seasonality characteristics and catchment characteristics.

In practice, models like the least-squares method (Li et al., 2013), the multiple stepwise regression model (Zhang et al., 2004; Yang et al., 2009), and the neural network model (Xu et al., 2013) are often developed to estimate the Budyko-type equation parameter by taking the influence factors as independent inputs. However, the water partitioning process is resulted from the hybrids of various influence factors (Milly, 1994; Yokoo et al., 2008; Gentine et al., 2012; Shao et al., 2012; Xu et al., 2013). Meanwhile, the influencing factors (i.e., climatic seasonality characteristics, catchment characteristics, and agricultural activities) have been widely recognized to be interconnected (Dietrich and Perron, 2006), which tends to reduce the range and variability of model response (Gentine et al., 2012; Liang et al., 2015). Therefore, investigation of the interactions between the influencing factors on the catchment-specific model parameter under a changing climate should urgently emerge for many disciplines such as hydrology, meteorology, and ecology. A nonparametric method, the multivariate adaptive regression spline (MARS) model proposed by Friedman (1991), is a powerful tool to identify important factors and their interactions by determining statistically significant factors. Recently, Shao et al. (2012) successfully applied the MARS model to estimate the Budyko parameter based on various climatic and catchment characteristics using 241 Australian catchments, where all the catchments have relatively small drainage areas without remarkable agricultural activities. Conversely, China is a vast agricultural country, with a plenty variety of catchments with cultivated and irrigated lands. This unique condition has caused the complicated and interconnected relationship in the water-energy controls of catchments. However, up to now, deterministic estimation of Budyko equation parameter based on various controls (especially the agricultural activities), and investigation of the interactions between influencing factors (i.e., climate, soil,

topography, vegetation properties and agricultural activities) across China are scarce.

Given that agricultural activities can also reflect the water partitioning across China, the ability of MARS model in determining statistically significant factors and their interactions, and the availability of selected 96 catchments data sets, in this study, the relationship between the "basin-specific" Budyko curves and their influencing factors, the correlations between the influencing factors are firstly detected by Pearson correlation analysis approach. The significant factors and their interactions is investigated by MARS model using data sets that span a wide range of climate regimes and spatial scales. More specifically, the influencing magnitudes of the interactions on the Budyko parameter estimation in different catchments, and the performances of MARS model compared to the parametric model (multiple stepwise regression model, taken the influencing factors as independent inputs) are also assessed.

2. Methodology

2.1. Budyko-type equation

The dynamic water balance equation of a natural watersheds is

$$\frac{d}{dt}S(t) = P(t) - E(t) - Q(t) \tag{1}$$

where $S(t)$ is the total stored water of the watershed, $P(t)$, $E(t)$, and $Q(t)$ are precipitation, evapotranspiration and runoff, respectively. For a watershed with irrigation, if the drainage area is large enough and there is no exchange between watersheds, the irrigation (I) at time t can be taken as the water demand from the runoff at time t-1. Accordingly, the irrigation (I) at time t can be taken as the water supply (as well as P at time t). The dynamic water balance of a catchment with agricultural activities terms as

$$\frac{d}{dt}S(t) + \frac{d}{dt}I(t) = P(t) - E(t) - Q(t) \tag{2}$$

Over a time interval T, Eq. (2) can be obtained as

$$\frac{S(T) - S(0) + I(T) - I(0)}{T} = P - E - Q \tag{3}$$

If T is long enough, e.g., decades, the storage and water utilization by irrigation terms (which are all from the P of the catchment) can be neglected and Eq. (3) becomes

$$0 = P - E - Q \tag{4}$$

That is, at the multi-year scale, the water utilization by agricultural activities in a catchment would not affect the water balance. Therefore, Budyko-type equations can also be used to assess the impacts of anthropogenic modifications on instream flow changes. Several mathematical equations have been developed to represent the Budyko framework and here the Choudhury equation (Choudhury, 1999) is used.

$$\frac{E}{P} = \frac{\frac{E_0}{P}}{\left[1 + \left(\frac{E_0}{P}\right)^n\right]^{1/n}} \tag{5}$$

where n is a catchment-specific parameter, which determines the evapotranspiration ratio (E/P) for given E_0/P, and modifies the partitioning of P between E and Q.

Daily E_0 is calculated based on the Penman equation that includes wind speed, relative humidity, air temperature, and radiation. The E_0 calculation follows Shuttleworth (1993):

$$\lambda E_0 = \frac{\Delta}{\Delta + \gamma}(R_n - G) + \frac{\gamma}{+\gamma}6.43(1 + 0.536U_2)\left(\frac{100 - RH}{100}\right)e_s \tag{6}$$

where E_0 is the potential evapotranspiration (mm d^{-1}); Δ is the slope of the vapor pressure curve (kPa $°C^{-1}$); γ is the psychrometric constant (kPa $°C^{-1}$); R_n is the net all-wave radiation at surface (MJ m^{-2} d^{-1}); G is the all-wave ground heat flux (MJ m^{-2} d^{-1}); U_2 is the daily average wind speed at 2-m height (m s^{-1}); RH is the relative humidity (%); and e_s is the saturated vapor pressure (kPa).

2.2. Influencing factors description

Catchment characteristics (including percentage of vegetation coverage, M; relief ratio, Rr; plant available water storage capacity, PAWC in mm), climatic seasonality characteristics (including average storm depth, ASD in mm; precipitation concentration index, CI; coefficient of variation of precipitation, Cv; seasonality index of precipitation, SI; Palmer drought severity index, PDSI; Milly's index of seasonality which is the number of months that peak precipitation follows peak potential evapotranspiration, SIM; number of months that peak precipitation follows peak potential evapotranspiration where the peaks were found from fitted sine functions based on the observed data, PfE), agricultural activities (including the percentage of irrigation area to the total catchment area, IA; the percentage of cultivated land area to the total catchment area, CA) in total 12 factors were selected in this work and their calculation methods are briefed in Table 1.

2.3. Multivariate adaptive regression spline model

In statistics, multivariate adaptive regression splines (MARS) is a form of regression analysis introduced by Friedman (1991). It is a non-parametric regression technique and can be seen as an extension of traditional linear regression models that automatically models nonlinearities and interactions between variables.

The objective of non-parametric regression is to estimate the regression function $f(\cdot)$ given by:

$$n = f(\mathbf{x}) + \varepsilon = f(x_1, \cdots, x_k) + \varepsilon \tag{7}$$

where $f(\cdot)$ is a function to be specified and $\mathbf{x} = \{x_1, \cdots, x_k\}$ is the collection of potential variables affecting the Budyko parameter n of Eq. (5).

MARS builds models of the form:

$$\hat{f}(\mathbf{x}) = \sum_{j=1}^{J} a_j b_j(\mathbf{x}) \tag{8}$$

where $\hat{f}(\mathbf{x})$ is the spline approximation of the function of interest $f(\mathbf{x})$; a_j is the coefficient of jth basis function $b_j(\mathbf{x})$, which can be considered weight that represents the importance of the jth variable.

Each basis function $b_j(\mathbf{x})$ is consisted by: 1) A constant. There is only one such term called the intercept. Note that this constant represents the possible intercepts in other basis functions. 2) A hinge function, has the form of $max(0, x - \text{knot})$ or $max(0, \text{knot} - x)$. MARS automatically selects variable x and values of those variables for knots of the hinge functions. 3) A product of two or more hinge functions.

In mathematics, the basis functions of MARS model (8) are in the form of

$$B_j(\mathbf{x}) = \prod_{i=1}^{K_j}[u_{ij} \cdot (x_{v(i,j)} - t_{ij})]_+ \tag{9}$$

where $u_{ij} = +1$ or $u_{ij} = -1$; $[z]_+$ is a truncated function of $\begin{cases} [z]_+ = z, \text{if} z \geqslant 0 \\ [z]_+ = 0, \text{if} z < 0 \end{cases}$; $x_{v(i,j)}$ represents a variable in $\mathbf{x} = \{x_1, \cdots, x_k\}$ (i.e., $v(i,j) \in \{1, \cdots, k\}$) which will be determined in MARS, t_{ij} give

Table 1
Calculation methods description for 14 influencing factors.

Budyko parameter influencing factors		Calculation methods	Equation description	Refs.
Catchment characteristics	Vegetation coverage (M)	$M = \frac{NDVI - NDVI_{min}}{NDVI_{max} - NDVI_{min}} \times 100\%$	NDVI min and NDVI max are chosen to be 0.05 and 0.8, respectively	Yang et al. (2009)
	Relief ratio (Rr)	$Rr = \frac{E_{high} - E_{low}}{L_{max}}$	The ratio of the catchment relief (i.e., the difference between maximum and minimum elevations) and the longest flow path	Shao et al. (2012)
	Plant available water storage capacity (PAWC, mm)	$PAWC = \int^{(} DUL - CLL) \times depthinterval$	DUL and CLL are drained upper limit and crop lower limit, respectively	McKenzie et al. (2003)
Climatic seasonalitycharacteristics	Average storm depth (ASD, mm)	$ASD = \frac{\sum_{j=1}^{N} \max(P_{i,j})}{N}$	$P_{i,j}$ is the precipitation of ith day in jst year; N is the total number of years	Bonta (2004)
	Precipitation concentration index (CI)	$CI = S/5000$	S is the surface area of the lower triangle delimited by the equidistribution line	Martin-Vide (2004)
	Coefficient of variation of precipitation (Cv)	$Cv = \frac{\sigma}{\bar{P}}$	σ and $\bar{P}$ are standard deviation and average for annual P	Ananthakrishnan and Soman (1989)
	Seasonality index of precipitation (SI)	$SI_i = \frac{1}{R_i} \sum_{n=1}^{12} \lvert X_{in} - \frac{R_i}{12} \rvert$	SI_i is the seasonality index of precipitation in the ith year; X_{in} is the precipitation of nth month in the ith year, mm; R_i is the precipitation of the ith year, mm	Walsh and Lawler (1981)
	Palmer drought severity index (PDSI)	$PDSI = f(P, T)$	PDSI is computed using observed or model monthly surface air temperature and precipitation	Palmer (1965)
	Milly's index of seasonality which is the number of months that peak precipitation follows peak potential evapotranspiration (SIM) The number of months that peak precipitation follows peak potential evapotranspiration (PfE) where the peaks were found from fitted sine functions based on the observed data	$P(t) = \bar{P}\{1 + \delta_P \sin(\omega_P t + \alpha_P)\}$ $E_0(t) = \bar{E_0}\{1 + \delta_{E_0} \sin(\omega_{E_0} t + \alpha_{E_0})\}$ $SIM = \lvert \delta_P - \delta_{E_0} DI \rvert$	ω_P and ω_{E_0} are the angular velocity of seasonal precipitation and potential evaporation, respectively, with $2\pi/\omega$ equal to one year; α_P and α_{E_0} are the phase difference from a standard time, 0-2π; δ_P and δ_{E_0} are the ratios of the amplitudes of the annual harmonics to the annual averages of P and E_0, respectively; DI is the climate drought index ($DI = E_0/P$)	Milly (1994); Woods (2003),
Anthropogenicfactors	Effective irrigated area ratio (IA)	$IA = \frac{\int^{A_i} S_i \cdot IA_i}{S_C} \times 100\%$	$\frac{A_i}{S_i}$ is the proportion of catchment located in the ith province, IA_i and CA_i are the total irrigated area, and cultivated land area of the ith province, respectively. S_C is the area of the catchment.	
	Cultivated land area ratio (CA)	$CA = \frac{\int^{A_i} S_i \cdot CA_i}{S_C} \times 100\%$		

the corresponding knot points at which the basis functions change, and K_j is the number of interacting variables in the basis function.

The aim of MARS is not only to adjust the coefficient values to best fit the data but also to derive a good set of basis functions based on the data. The best model is determined by the generalized cross validation criterion (GCV), which is an alternative to having both training data sets, and overfit checking data sets for model validation, is given by:

$$\mathrm{GCV}(\lambda) = \frac{\sum_{i=1}^{N} (y_i - \hat{f}_\lambda(x_i))^2}{(1 - M(\lambda)/N)^2} \tag{10}$$

where $\hat{f}_\lambda$ is the estimate based on λ basis functions; and $M(\lambda)$ is a complexity cost function.

MARS builds a model in two phases: the forward and the backward pass. The forward pass usually builds an overfit model, the terms keep added until the maximum GCV value is reached (that is, any more term will reduce the GCV value). The model after the forward selection is called the full model. Backward selection tends to eliminate the less important terms which reduce the GCV values. The backward step starts from the full model and a term which is least important (that is the GCV value will increase mostly without this term) is then removed. The terms keep removed until the maximum GCV value is reached. The model after the backward selection is called the final model.

In this paper, only the first order interaction is considered, i.e., we limit the MARS model to pairwise interactions, in order that it is able to manifest the hydrological interpretations for the model components.

2.4. Measures of performance assessment

Performance of the MARS model for estimating n is evaluated by comparing estimated n against n values calculated by Eq. (5) using the observations. Two statistics, namely the correlation coefficient (R), and mean absolute errors (MAE) are used to evaluate the performance of MARS model and are defined in the form as:

$$R = \frac{\sum_{i=1}^{m} (O_i - \bar{O})(S_i - \bar{S})}{\left[\sum_{i=1}^{m} (O_i - \bar{O})^2\right]^{0.5} \left[\sum_{i=1}^{m} (S_i - \bar{S})^2\right]^{0.5}} \tag{11}$$

$$MAE = \frac{\sum_{i=1}^{m} (S_i - O_i)}{m} \tag{12}$$

with $\bar{O} = \sum_{i=1}^{m} O_i/m$ and $\bar{S} = \sum_{i=1}^{m} S_i/m$ are the average of the observed variable O_i and the average of the simulated variable $S_i (i = 1, 2, \ldots, m)$, respectively, where m is the number of space-steps.

3. Study area and data processing

Spanning different climatic conditions, a total of 96 catchments (including catchments in Songhua River basin, Liao River basin, Hai River basin, Yellow River basin, Huai River basin, Yangtze River basin, Pearl River basin, Yalungzangbo River basin, etc) selected in this study are from China. The location map of these selected catchments is given in Fig. 1. Meanwhile, the detailed information for discharge control gauges from 96 catchments (selected based on the data availability and quality), including the longitude, latitude and the drainage area that each gauge controlled, are shown in Table 2.

To ensure each catchment has at least 10 complete years of unimpaired streamflow data, we collected monthly streamflow data from most of the 96 discharge control gauges covering the 1981–2000 period, and the gauges in the Tibet from the recorded year to 2010 period. The streamflow data were collected from the Ministry of Water Resources, China. The missing data accounts for less than 1% of the total data and were processed using the 5-year moving average method.

Daily meteorological data, such as precipitation, maximum and minimum temperature, wind speed and relative humidity, were collected from 412 stations (can be seen in Fig. 1) covering the same period as the observed streamflow data. The meteorological data was obtained from the Climatic Data Center, National Meteorological Information Center, China Meteorological Administration. The procedure for calculating the catchment average climatic variables are as follows: (1) a 10 km grid data set covering the study areas was interpolated from the weather stations data; (2) potential evaporation was estimated in each grid; and (3) the catchment average values were calculated. Air temperature was interpolated using an inverse-distance weighted technique that considers the effect of elevation. Other variables were interpolated using an inverse-distance weighted technique.

For each of the catchments, information about land use, topographic characteristics, and soil properties was also obtained. The topographic data came from 30 m resolution digital elevation maps. The soil properties include upper and lower soil-horizon soil moisture content, soil types, and depths of A and B horizons, were from the ORNL DAAC (Oak Ridge National Laboratory Distributed Active Archive Center) (https://daac.ornl.gov/soils). NDVI (1981–2000; spatial resolution 0.073°) data set was acquired from the GIMMS (Global Inventory Modeling and Mapping Studies) (http://glcf.umd.edu/data/gimms). In addition, the agricultural activities (i.e., IA and CA) data were sourced from National Bureau of Statistics of China (http://data.stats.gov.cn).

4. Results

4.1. Basin-Specific Budyko parameter

Using long-term mean annual Q, P, and E_0 data, Budyko parameter n for "specific basin" was obtained by Eq. (5). Fig. 2(a) presents the spatial distribution of Budyko parameter n values. The Budyko curves with different n values range from 0.301 to 3.047, repre-

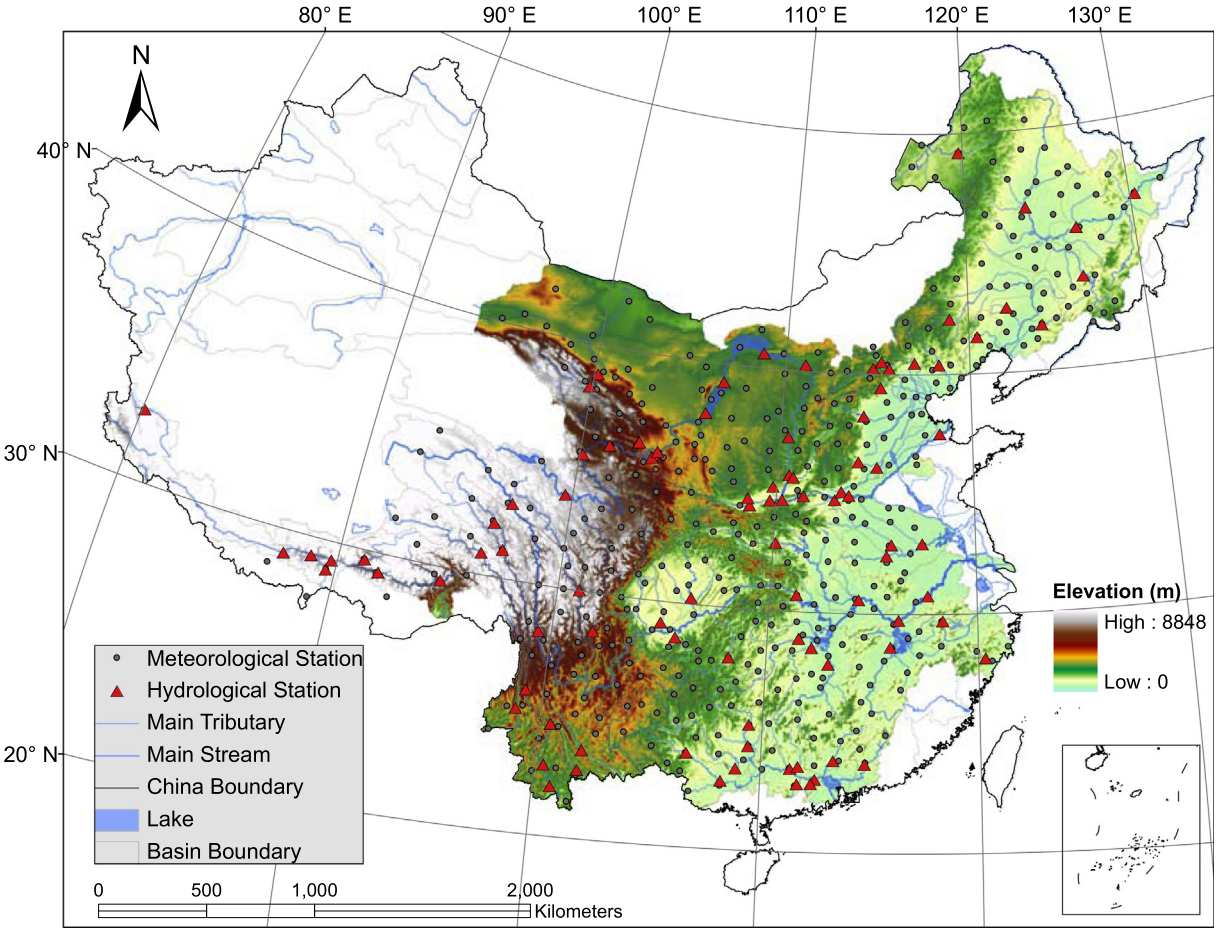

Fig. 1. Location of meteorological stations, hydrological stations and catchments used in this study.

Table 2
Location information and hydro-climatic characteristics of the 96 catchments used in this study.

Catchment	River	Hydrological station	Longitude (°E)	Latitude (°N)	Drainage area (km^2)	Catchment	River	Hydrological station	Longitude (°E)	Latitude (°N)	Drainage area (km^2)
Songhua River basin	Second Songhua River	Fengman Reservoir	126.67	43.73	42,500	Yangtze River basin	Ya-lung River	Luning	101.87	28.45	108,083
	Mainstream	Harbin	126.58	45.77	389,769		Chishui River	Chishui	105.68	28.58	16,622
	Mainstream	Jiamusi	130.32	46.80	528,277		Tuo River	Lijiawan	104.95	29.13	22,472
	Nen River	Jiangqiao	123.68	46.78	162,569		Jialiang River	Wusheng	106.27	30.27	79,714
Hailaer River basin	Mainstream	Hailaer	119.75	49.20	22,516		Wu River	Xinan	108.25	27.95	51,270
Liao River basin	Liu River	Naodehai Reservoir	122.17	42.68	4051		Mainstream	Yichang	111.28	30.70	1,005,500
	Hun River	Dahuofang Reservoir	124.08	41.88	5437		Yuan River	Taoyuan	111.48	28.90	85,223
	West Liao River	Chifeng	118.93	42.28	8678		Zishui River	Taojiang	112.12	28.53	26,748
Daling River basin	Mainstream	Chaoyang	120.45	41.53	10,236		Xiang River	Xiangtan	112.92	27.87	81,638
Hai River basin	Luan River	Panjiakou Reservoir	118.30	40.40	33,700		Bai River	Baihe	110.12	32.82	59,115
	Chaobai River	Miyun Reservoir	116.98	40.47	9027		Mainstream	Hankou	114.28	30.58	1,488,036
	Sanggan River	Shixiali	114.73	40.25	23,944		Gan River	Waizhou	115.83	28.63	80,948
	Yang River	Xiangshuibao	115.18	40.52	14,507		Poyang Lake	Hukou	116.22	29.75	162,225
	Yongding River	Guanting Reservoir	115.60	40.23	42,500		Mainstream	Datong	117.62	30.77	1,705,383
	Hutuo River	Huangbizhuang Reservoir	114.30	38.25	23,000	Xin'anRiver basin	Mainstream	Tunxi	118.33	29.72	2670
	Zhang River	Guantai	114.08	36.33	17,800	OuRiver basin	Mainstream	Weiren	120.33	28.15	13,500
	Daqing River	Zijingguan	115.17	39.43	1760	PearlRiver	West River	Wuzhou	111.33	23.47	327,006
	Wei River	Yuancunji	115.05	36.12	14,286	basin	East River	Heyuan	114.70	23.73	15,750
Yellow	Mainstream	Jimai	99.65	33.77	45,019		North River	Hengshi	113.27	23.85	34,013
River	Mainstream	Tangnaihai	100.15	35.50	121,972		Liu River	Liuzhou	109.40	24.33	45,413
basin	Mainstream	Guide	101.40	36.03	133,650		Yu River	Nanning	108.23	22.83	72,656
	Huangshui River	Minhe	102.80	36.33	15,342		West River	Gaoyao	112.47	23.05	351,535
	Datong River	Xiangtang	102.83	36.35	15,126		He River	Gulan	111.68	23.57	8273
	Tao River	Hongqi	103.57	35.80	24,973		Qingshui River	Zouwei	108.88	23.38	1896
	Mainstream	Lanzhou	103.82	36.07	222,551		Rong River	Chang'an	109.38	25.22	21,530
	Mainstream	Qingtongxia	106.00	37.90	275,010		You River	Baise	106.63	23.90	21,720
	Mainstream	Shizuishan	106.78	39.25	309,146		Luoding River	Guanliang	111.67	22.83	3164
	Mainstream	Sanhuhekou	108.77	40.62	347,909		Xinxing River	Yaogu	112.28	22.87	1776
	Mainstream	Hekou	111.07	40.27	367,898	HeiRiver basin	Mainstream	Yingluoxia	100.18	38.80	10,009
	Wuding River	Baijiachuan	110.42	37.23	29,662		Babao River	Qilian	99.87	38.25	2452
	Mainstream	Longmen	110.58	35.67	497,561	Yalungzangbo	Lhasa River	Lhasa	91.15	29.63	26,235
	Fen River	Hejin	110.80	35.57	38,728	Riverbasin	Nianchu River	Shigatse	88.83	29.30	11,101
	Wei River	Xianyang	108.70	34.28	49,800		Nianchu River	Jiangzi	89.60	28.90	6216
	Wei River	Huaxian	109.70	34.56	105,350		Mainstream	Lazi	87.65	29.12	47,832
	Jing River	Zhangjiashan	108.58	34.58	41,800		Mainstream	Nugesha	89.75	29.30	106,060
	North Luo River	Zhuangtou	109.80	35.13	26,700		Mainstream	Yangcun	91.87	29.27	152,701
	Mainstream	Tongguan	110.30	34.62	682,166		Mainstream	Nuxia	94.65	29.47	191,235
	Mainstream	Sanmenxia	111.37	34.82	688,421	LancangRiver	Mainstream	Changdu	97.17	31.13	54,228
	Yiluo River	Heishiguan	112.93	34.72	18,563	basin	Heijiang River	Daxinshan	100.40	22.87	8749
	Qin River	Wuzhi	113.27	35.07	12,880		Zhaqu River	Xiangda	96.57	32.13	17,909
	Mainstream	Huayuankou	113.65	34.92	730,036		Mainstream	Gajiu	100.50	24.53	108,527
	Mainstream	Lijin	118.30	37.53	751,869		Mainstream	Jiuzhou	99.22	25.78	84,220
Huai River basin	Mainstream	Wangjiaba	115.60	32.43	30,630		Mainstream	Yunjinghong	100.78	22.03	142,963
	Ying River	Fuyang	115.83	32.90	35,246	RedRiver basin	Yuan River	Yuanjiang	102.00	23.62	21,554
	Mainstream	Bengbu	117.37	32.95	121,330		Lixian River	Lixianjiang	101.87	22.80	16,524
Yangtze River basin	Mainstream	Zhimenda	97.23	33.02	137,704	NuRiver basin	Mainstream	Jiayuqiao	96.23	30.87	72,844
	Jiaojie River	Shangqiaotou	99.40	28.17	2432		Mainstream	Daojieba	98.88	24.98	110,224
	Ya-lung River	Yajiang	101.02	30.03	66,871	IndusRiver basin	Mainstream	Shiquanhe	80.10	32.50	12,297

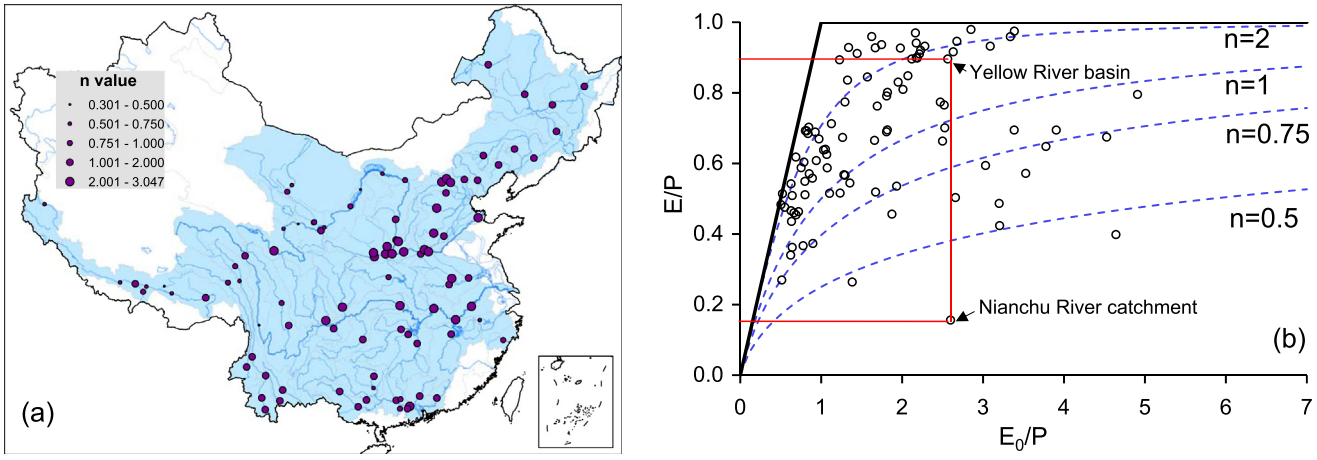

Fig. 2. (a) Spatial distribution of Budyko parameter *n*, (b) Mean annual evaporation ratio (E/P) versus mean annual arid index (E_0/P). The Budyko curves calculated by Eq. (1) are plotted as dash lines with the fitted *n* values.

senting the complexity of the regional climate and catchment characteristics. The distribution has a clear spatial structure with low *n* values in the western catchments (upper reaches of Yellow River and Yangtze River, catchments in Tibet) and high ones in the eastern catchments (Hai River basin, Huai River basin, lower reaches of Yellow River and Yangtze River, and Pearl River Delta). The long-term mean annual evapotranspiration ratio (E/P) versus dryness index (E_0/P) for 96 catchments of different climatic conditions are plotted in Fig. 2(b). It is evident that for certain dryness index, E would increase with larger parameter *n*. Taking the middle reach of Yellow River basin (controlled by Longmen gauge) and Nianchu River catchment (controlled by Jiangzi gauge) as a paired example, although the similar climatic conditions of the middle Yellow River basin (with E_0/P = 2.562) and the Nianchu River catchment (with E_0/P = 2.597), the evapotranspiration ratios (E/P) are quite different with 0.896 and 0.156, respectively for the different parameters *n* values (1.690 and 0.301). Fig. 2(a) and (b) also demonstrate that most *n* values of catchments range from 0.5 to 2.5, accounting 82.3% of all catchments.

4.2. Spatial distribution of influencing factors

The distributions of catchment characteristics (i.e., M, Rr and PAWC) are shown in Fig. 3. The Pearl River basin, southern catchments of China are covered by high vegetation cover, while respectively low M values are located in the upper and middle reaches of Yellow River basin, Hei River basin and Brahmaputra River basin (Fig. 3(a)). Rr represents the topographic controls on parameter *n* of the catchment, which ranges from 0.001 to 0.026 (Fig. 3(b)), the most cliffy catchments are located in the Tibetan Plateau and Yunnan-Guizhou Plateau. Fig. 3(c) illustrates that high PAWC values are distributed in the middle and lower reaches of Yangtze River basin, Pearl River basin.

As for the climatic seasonality characteristics, the distributions are presented in Fig. 4. High ASD and CI values are located on the southern catchments (Fig. 4(a) and (b)), while high Cv and SI values are distributed on the northern catchments (including Songhua River basin, Liao River basin, Hai River basin, northern Yellow River basin, and Yalungzangbo River basin) (Fig. 4(c) and (d)). Fig. 4(e) replays that low PDSI values are distributed on the Yellow-Huai-Hai region. Most SIM values are smaller than 3, while high SIM values are located on the Hei River basin and the middle region of Yellow River (Fig. 4(f)). Fig. 4(g) depicts that lower PfE values are distributed on the Hei River basin, the source regions of Yellow River and Yangtze River, the Lancang River basin.

Fig. 5 demonstrates the spatial distributions of agricultural activities (i.e., IA and CA) density. It can be concluded that IA and CA are subject to huge spatial heterogeneity within 96 catchments across China. We found that the higher IA and CA ones are distributed on the Hai River basin, Huai River basin, Xin'an River basin, Ou River basin, Pearl River basin and the lower reaches of Yellow River basin, Yangtze River basin.

Overall, the spatial variabilities in climate, catchment characteristics and agricultural activities further confirms the hetero-

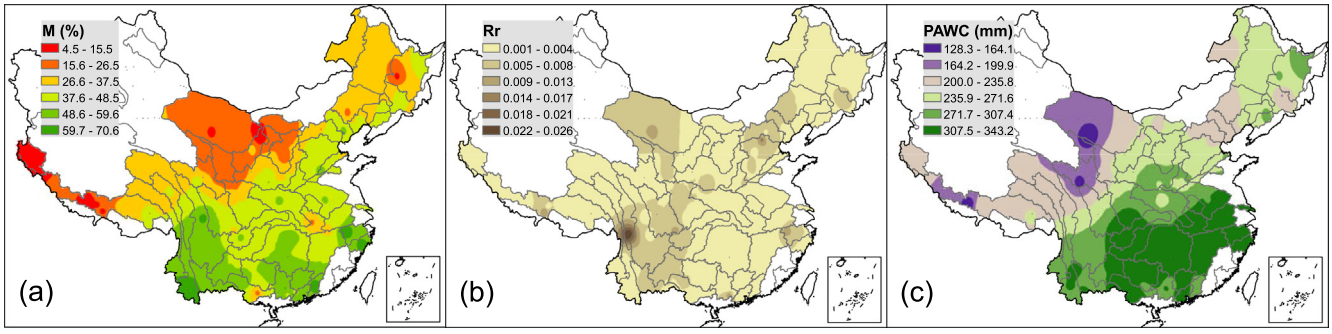

Fig. 3. Spatial distribution of (a) M, (b) Rr, and (c) PAWC across selected 96 catchments of China.

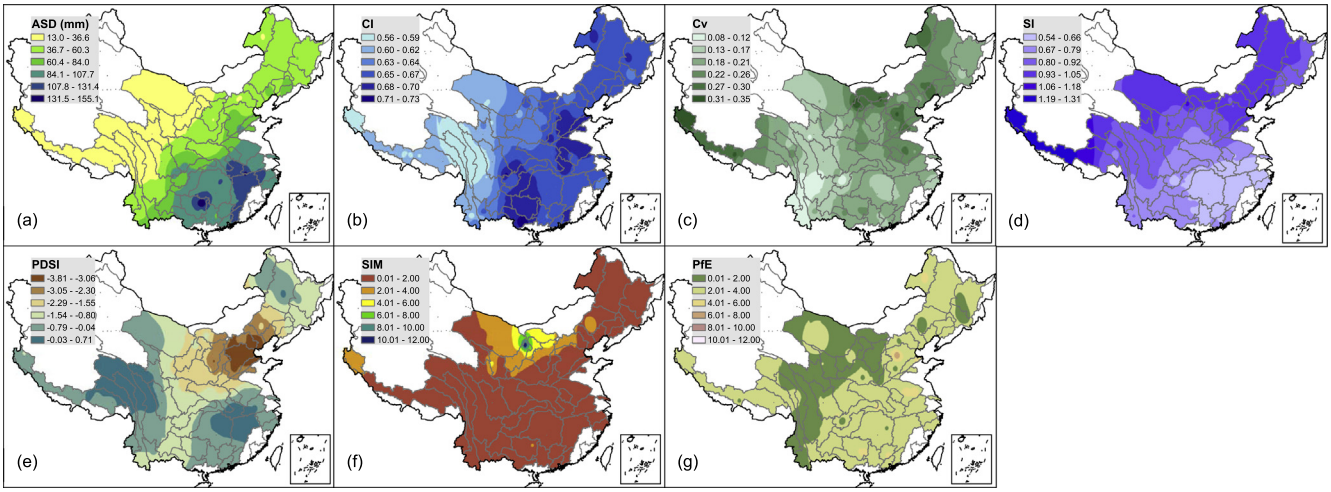

Fig. 4. Spatial distribution of (a) ASD, (b) CI, (c) Cv, (d) SI, (e) PDSI, (f) SIM, and (g) PfE across selected 96 catchments of China.

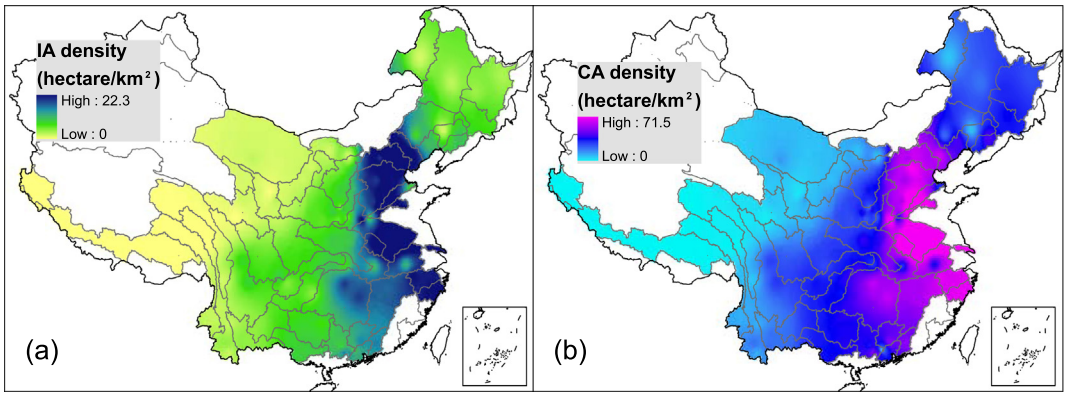

Fig. 5. Spatial distribution of (a) IA density, and (b) CA density across selected 96 catchments of China.

geneities in Budyko curves between multiple catchments. This may not be surprising, as evapotranspiration is a very complex random processes influenced by various natural and anthropogenic factors.

4.3. Correlation of Budyko parameter and the influencing factors

Before employing the MARS model to estimate the Budyko parameter n, the correlations between the Budyko parameter n and influencing factors are investigated by Pearson correlation analysis (see Table 3). It can be seen that except Cv and PfE have insignificant correlation with Budyko parameter n spatially change, other factors, especially soil properties (i.e., PAWC), climatic seasonality characteristics (i.e., ASD, CI, SI and PDSI) and agricultural activities (i.e., IA and CA) have close relationships (the absolute correlation coefficients over 0.3) with Budyko parameter n spatially change. Furthermore, the multiple stepwise regression (MSR) model, a widely used method to identify the dominant variables associated with the Budyko parameter (Zhang et al., 2004; Yang et al., 2009), was employed to possibly explain the underlying mechanisms of n spatially change by considering the Budyko parameter n spatially series as a dependent variable and 12 influencing factors as independent variables. A total of five out of 12 explanatory variables were selected in the final MSR model for the 96 typical catchments, the final model is as follows:

Table 3
Correlation of influencing factors and Budyko parameter n by Pearson correlation analysis.

	Pearson correlation	Sig. (2-tailed)	Sig. level
M	0.208	0.0416	0.05
Rr	−0.225	0.0279	0.05
PAWC	0.357	0.0004	0.01
ASD	0.346	0.0006	0.01
CI	0.424	0.0000	0.01
Cv	−0.004	0.9703	No significant
SI	−0.320	0.0015	0.01
PDSI	−0.358	0.0003	0.01
SIM	−0.259	0.0109	0.05
PfE	0.163	0.1117	No significant
IA	0.361	0.0003	0.01
CA	0.362	0.0003	0.01

$$n = 2.100 * CI - 0.157 * SIM - 0.284 * PDSI - 1.203 * SI - 45.4 * Rr + 1.299 \quad (13)$$

This model explains 42.6% of observed variance with R of 0.653, MAE of 5.47 and with CI explaining 18.0%, SIM 6.8%, PDSI 7.7%, SI 5.2% and Rr 4.9% of variance. Although the MSR model (Eq. (13)) explains nearly half of the variance of the Budyko parameter n,

the predictive capacity of n is weak, particularly at the high end. Noticeably, although some factors are insignificant variables for Budyko parameter n spatially change, the interactions between the influencing factors can also have potential influence on the catchment-specific model parameter estimation.

4.4. Correlation between influencing factors

The correlation between influencing factors were also examined by Pearson correlation analysis, and the results are given in Table 4. Except Rr, CI and PDSI, all the other factors are significantly correlated with M. Most of these correlations are positive, while climatic seasonality characteristics (i.e., Cv, SI and SIM) have negative correlation with M. Only CI has significant negative correlation with Rr, which represents that steep slopes tend to generate more concentrated rainfall. The correlations of PAWC with most factors are significant and positive, only the correlations of Cv and SI with PAWC are negative. Overall, most of the correlations of climatic seasonality characteristics with catchment characteristics and agricultural activities factors are significant. This phenomenon further confirms that these influencing factors are interconnected, and potentially tend to affect the water partitioning process.

4.5. Interactions between variables identified by MARS

Instead of making a subjective selection, we kept all the 12 influencing factors and let the MARS model determine the statistically significant ones. 22 basis functions were initially selected as the full model after the forward selection (when the relative change of mean square errors reaches to 0.001) but only 14 basis functions remained after the backward selection. Table 5 lists the final 14 basis functions given by their coefficients and knot points of the selected variables, which are given by nonzero values. The final model with MSE = 0.119 and GCV = 0.213. The final 14 basis functions can be grouped into 8 sets of functional forms representing constant, functions for single variable and functions for the interaction between variables.

Detailed explanations are given below:

(1) The constant factor $f(\mathbf{x}) = 1.721$ described as the first term gives the baseline value of the Budyko parameter n.
(2) The effect described by terms 2 and 3 is ASD. The spline function is given as

$$f_{ASD} = -0.0372[-(ASD - 46.78)]_+ - 0.0061[+(ASD - 46.78)]_+ + 1.721 \quad (14)$$

and is plotted together with observed values in Fig. 6(a). It can be seen from Fig. 6(a) that when ASD < 46.78 mm, f_{ASD} = −0.0372 × (46.78-ASD), mostly occurs in the northwestern arid catchments (seen in Fig. 4(a)). This means higher ASD across the northwestern arid region would have a higher evapotranspiration ratio, this phenomenon illustrates that the rainfall is preferred to evaporate in the arid catchments. In the semi-humid and humid regions with larger ASD (>46.78 mm), the rainfall will generate runoff first. Especially for some low-lying and landlocked areas, the

Table 4
Correlation between influencing factors by Pearson correlation analysis.

	M	Rr	PAWC	ASD	CI	Cv	SI	PDSI	SIM	PfE	IA	CA
M												
Rr	0.057											
PAWC	0.537**	−0.119										
ASD	0.471**	−0.166	0.763**									
CI	0.130	−0.228*	0.496**	0.701**								
Cv	−0.407**	−0.082	−0.255*	−0.051	0.264**							
SI	−0.614**	0.077	−0.769**	−0.692**	−0.350**	0.510**						
PDSI	0.082	−0.072	0.122	0.130	−0.346**	−0.307**	−0.235*					
SIM	−0.367**	−0.087	0.170	−0.145	0.006	0.402**	0.287**	−0.178				
PfE	0.219*	−0.047	0.246*	0.471**	0.372**	0.342**	0.162	0.051	0.270*			
IA	0.385**	0.008	0.317**	0.486**	0.443**	0.139	−0.315**	−0.323**	−0.106	0.309**		
CA	0.420**	−0.048	0.416**	0.565**	0.508**	0.120	−0.398**	−0.267**	−0.143	0.339**	0.958**	

Note: number with "**" and "*" indicate the correlation are significant at the level of α = 0.01 and 0.05 determined by Pearson correlation analysis.

Table 5
Full multivariate adaptive regression spline (MARS) model with the final model indicated by nonzero coefficients[a].

Basis	Coefficient	M	Rr	PAWC	ASD	CI	Cv	SI	PDSI	SIM	PfE	IA	CA
1	1.721												
2	−0.0061				1(46.78)								
3	−0.0372				−1(46.78)								
4	−0.027	1(34.56)											
5	−0.030	−1(34.56)											
6	−1.518							1(0.797)					
7	−3.743							−1(0.797)					
8	0.0013				1(46.78)								−1(21.97)
9	0.0002				1(46.78)								1(21.97)
10	−0.918							1(0.797)	−1(−0.740)				
11	−5.43						−1(0.230)	−1(0.797)					
12	−3.74						1(0.140)	1(0.797)					
13	0.0037	−1(34.56)										1(4.34)	
14	0.0079	−1(34.56)										−1(4.34)	

[a] Each row represents a MARS term in which the factor having 1 indicates the form $(x - t)_+$ (i.e., x > t), −1 indicates the form $(t - x)_+$ (i.e., x < t) and 0 indicates not in the model. The knot points t are given in parentheses. The first row without any nonzero knot provides the constant factor or baseline. The factors without entries are not selected in the final model. The basis functions are grouped (by solid line) in order to form appropriate functional form for easy explanation.

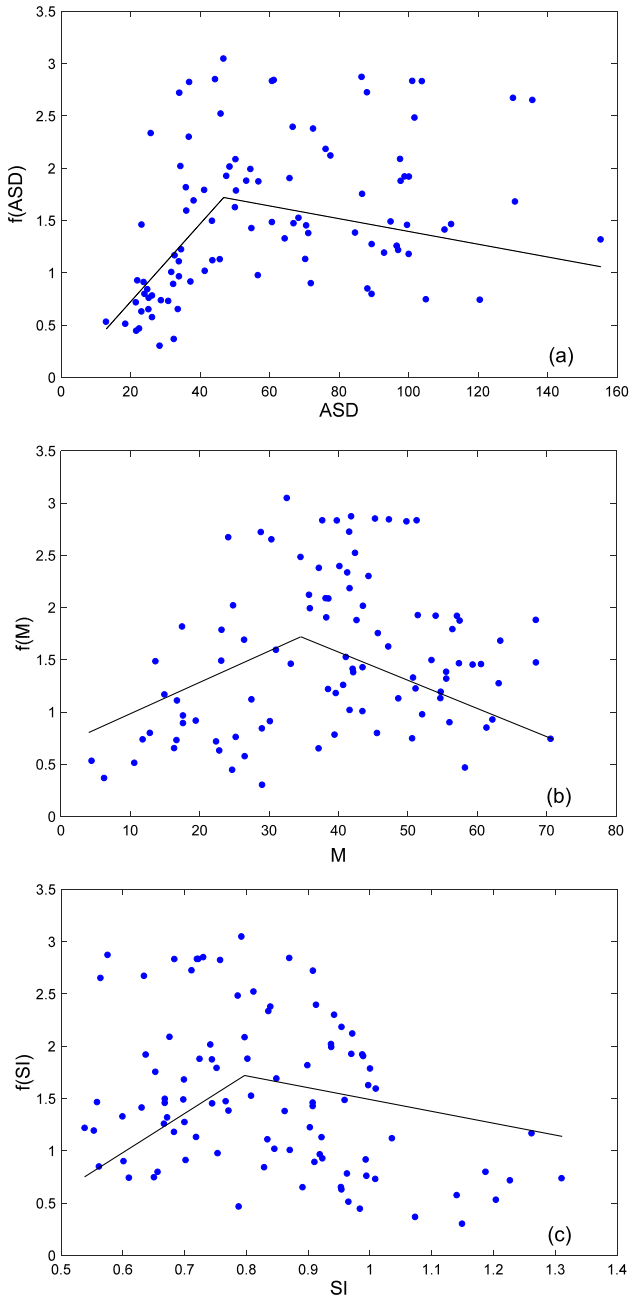

Fig. 6. Plot of effect for single variable (a) ASD, (b) M, and (c) SI on the Budyko parameter n in the MARS model. The blue dots represent the Budyko parameter n values calculated by Eq. (5).

intense rain cannot be quickly released to cause the excessive saturation of farmland water and soil moisture, likely resulting in more geological disasters.

(3) The effect depicted by terms 4 and 5 is M and is given in Fig. 6(b). The spline function is given as

$$f_M = -0.030[-(M-34.56)]_+ - 0.027[+(M-34.56)]_+ + 1.721 \quad (15)$$

Fig. 6(b) shows that when M > 34.56, the catchments locating in the Pearl River basin, southern of China (Fig. 3(a)) will have small Budyko parameter value and tend to generate more runoff. This result means that within a certain range, vegetation has the effect of weakening peak in flood process. Fig. 3(a) reveals that the catchments with less than 34.56% vegetation cover are located in the upper and middle reaches of Yellow River basin, Hei River basin and Brahmaputra River basin with the dryness index greater than 2.0 and the Budyko parameter value smaller than 1.0.

(4) The effect depicted by terms 6 and 7 is SI and is given in Fig. 6(c). The spline function is given as

$$f_{SI} = -3.743[-(SI-0.797)]_+ - 1.518[+(SI-0.797)]_+ + 1.721 \quad (16)$$

Fig. 6(c) demonstrates that the threshold value is 0.797 here in the equation, the Budyko parameter will increase when SI is less than 0.797. Only on the catchments of the southeastern China, which regions are covered by relatively low SI values (<0.797), would have increasing evapotranspiration ratios along with the increasing SI (Fig. 4(d)). While the northern catchments with relatively large SI are favorable for runoff generation and this leads to lower evapotranspiration ratios. SI represents the uneven distribution index of monthly rainfall in annual rainfall (see Table 1), Fig. 6(c) confirms that more decentralized rainfall can result more runoff generation.

We now investigate the interaction terms recognized by the MARS model.

(5) The first interaction is between CA and ASD (by terms 8 and 9). The spline function is given as

$$f_{CA,ASD} = +0.0013[-(CA-21.97)]_+[+(ASD-46.78)]_+ +0.0002[+(CA-21.97)]_+[+(ASD-46.78)]_+ + 1.721 \quad (17)$$

and is depicted in Fig. 7(a). This interaction term suggests that crop area with higher ASD tend to have higher evapotranspiration ratio, especially when the CA is relatively small. The correlation of CA and ASD is 0.565 (Table 4), it also can be seen from Figs. 4(a) and 5(d) that the CA density will increase with large ASD. By jointly viewing Figs. 4(a) and 7(a), we can conclude that although the effect of higher ASD (>46.78 mm, locating in the southeastern humid region) is to reduce the Budyko parameter value (Fig. 6(a)), for catchments with crops planting, this effect is undermined. Theoretically, this reduction should be enhanced when the CA increases. However, the rising evapotranspiration ratio by the higher ASD and smaller CA is found in Fig. 7(a), this bias in the data set is a likely cause of the inconsistent relationship for the catchments with high ASD and low CA.

(6) The second interaction is between PDSI and SI (by term 10). The spline function is given as

$$f_{PDSI,SI} = -0.918[-(PDSI+0.740)]_+[+(SI-0.797)]_+ + 1.721 \quad (18)$$

and is depicted in Fig. 7(b). It can be seen that the interaction between PDSI and SI is to reduce the Budyko parameter n when the PDSI is less than −0.740 and the SI is higher than 0.797. Fig. 4(d), (e) and (b) suggest that catchments in the Hai River basin, the Liao River basin and the middle and lower reaches of the Yellow River basin with lower PDSI but greater SI would have a low Budyko parameter n and a small evapotranspiration ratio. This result confirms that small PDSI (i.e., large dryness index) tends to enhance the Budyko parameter reduction by SI.

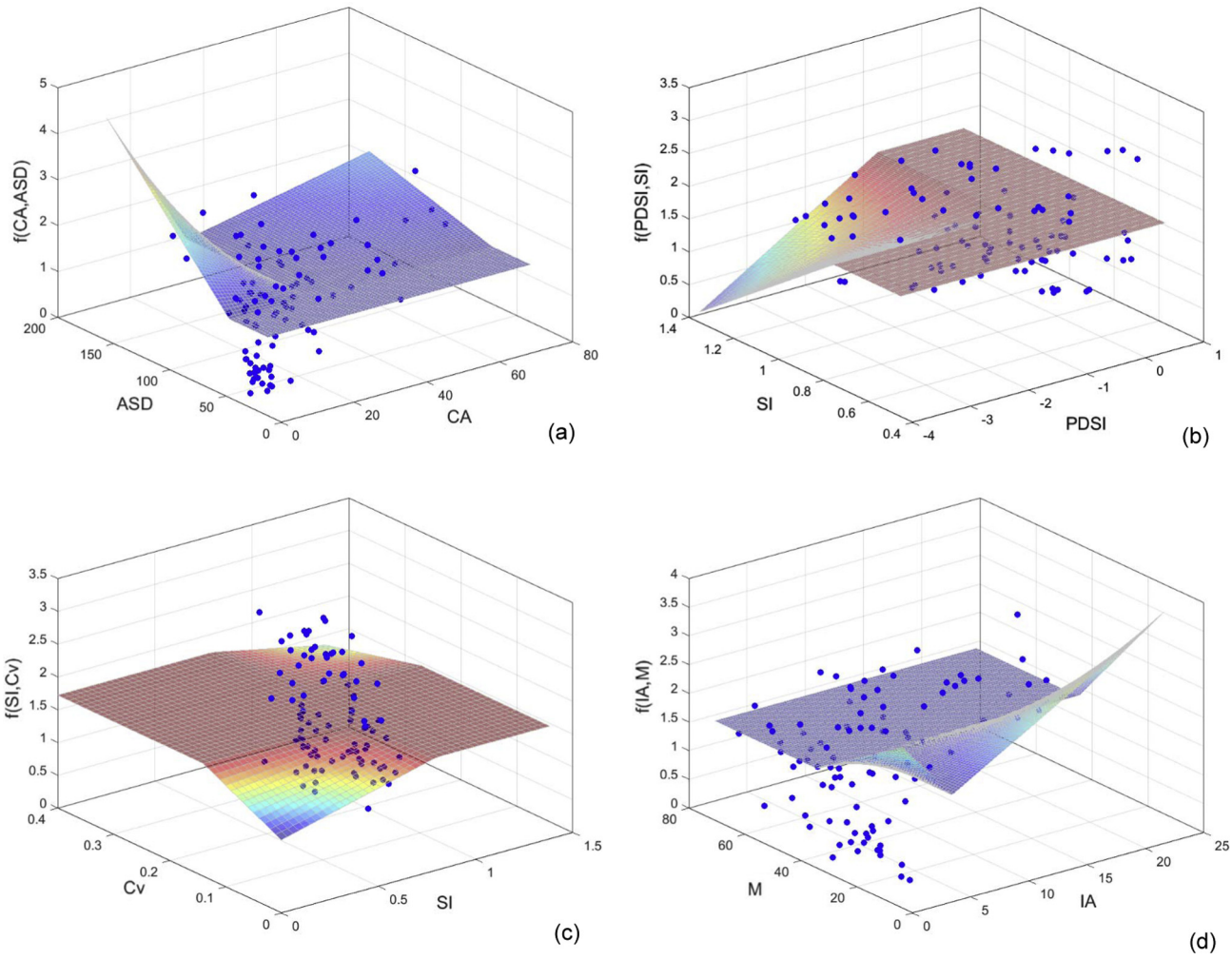

Fig. 7. Plot of effect of the interaction between (a) CA and ASD, (b) PDSI and SI, (c) SI and Cv, and (d) IA and M on the Budyko parameter n in the MARS model. The blue dots represent the Budyko parameter n values calculated by Eq. (5).

(7) The third interaction is between SI and Cv (by terms 11 and 12). The spline function is given as

$$f_{SI,Cv} = -5.43[-(SI - 0.797)]_+[-(Cv - 0.140)]_+ -3.74[+(SI - 0.797)]_+[+(Cv - 0.230)]_+ + 1.721 \quad (19)$$

and is depicted in Fig. 7(c). It can be seen that the Budyko parameter n value is small when the SI is less than 0.797 and the Cv is less than 0.14, or when the SI is larger than 0.797 and the Cv is higher than 0.23. This interaction term suggests that catchments with relatively large SI and Cv or catchments with small SI and Cv are favorable for runoff generation and therefore have lower evapotranspiration ratio. Fig. 4(c), (d) and (c) suggest that catchments in the Hai River basin, the middle and lower reaches of the Yellow River basin with high SI and Cv values, or catchments in the lower reach of Yangtze River basin, and southeastern catchments have low SI and Cv values would have a lower Budyko parameter n and generate more runoff.

The fourth interaction is between IA and M (by terms 13 and 14). The spline function is given as

$$f_{IA,M} = +0.0079[-(IA - 4.34)]_+[-(M - 34.56)]_+ +0.0037[+(IA - 4.34)]_+[-(M - 34.56)]_+ + 1.721 \quad (20)$$

and is depicted in Fig. 7(d). It can be seen that the Budyko parameter n value is higher when the IA is lower than 4.34% and M is lower than 34.56%, or when the IA is higher than 4.34% and M is lower than 34.56%. This interaction term suggests that catchments with low IA (<4.34) and M (<34.56) tend to generate less runoff and therefore have higher evapotranspiration ratio. By jointly viewing Figs. 6(b) and 7(d), we can conclude that low M enhances the rising effect on evapotranspiration ratio by the IA.

4.6. Assessment of MARS model's performance

Fig. 8 compares the calculated Budyko parameter n values by Eq. (5) using the observations and estimated ones by the MARS model for all the 96 catchments. Good agreement can be found with the correlation coefficient (R) is 0.817 and the mean absolute error (MAE) is 4.09. The MARS model performs better than the MSR model in term of Budyko parameter n, with higher explained variance (66.7% relative to 42.6%) and lower MAE (4.09 relative to 5.47). The encouraging result provides confidence in the MARS model to examine the interactions between climatic seasonality, catchment characteristics and anthropogenic factors to variations in the hydrological regime.

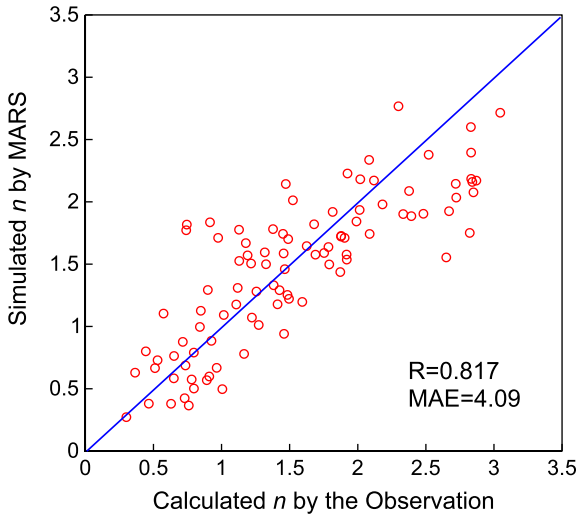

Fig. 8. Simulated Budyko parameter n by the MARS model and calculated ones by the observation for all catchments.

5. Discussion

5.1. Impacts of interactions between variables on Budyko parameter estimating

In our study, Pearson correlation shows that not only the soil properties (i.e., PAWC) and climatic seasonality characteristics (i.e., ASD, CI, SI and PDSI) but also agricultural activities factors (i.e., IA, and CA) have close relationship with Budyko parameter n spatially change (seen in Table 3). Most of the correlations between climatic seasonality characteristics and catchment characteristics, agricultural activities are significant (seen in Table 4). These results show that the influencing factors are interconnected, which potentially tend to affect the water partitioning process. In addition, CI, SIM, PDSI, Rr, and SI were selected as the significant variables by the MSR model (Eq. (13)). These influencing factors have also been proved to be useful for measuring climate changes and interventions in alteration of the water partitioning (Williams et al., 2012; Berghuijs et al., 2014; Monjo and Marin-Vide, 2016). However, estimating the Budyko parameter by the influencing factors as independent inputs can lead to incorrect conclusions on the relationship between Budyko parameter n and its influencing factors (Milly, 1994; Yokoo et al., 2008; Gentine et al., 2012; Shao et al., 2012; Xu et al., 2013). In this context, the MARS model was employed to identify important factors with consideration of their interactions on Budyko curves.

In the MARS model process, for our 96 collected catchments across China, there are three significant factors and different directions of linear regressions on the Budyko parameter, including ASD, M and SI, respectively (Table 5 and Fig. 6). In the semi-humid and humid regions with larger ASD, rain is preferred to generate runoff first, especially for some low-lying and landlocked areas, the intense rain cannot be quickly released to cause the excessive saturation of farmland water and soil moisture, likely resulting in more geological disasters. Within a certain range, vegetation has the effect of weakening the runoff extremum. SI, representing the uneven distribution index of monthly rainfall in annual rainfall confirms that more decentralized rainfall can result more runoff generation. Using 241 Australian catchments, Shao et al. (2012) found PfE is a significant term affecting the mean annual E, and the functional relationship of E with PfE stated that closer phase between precipitation and potential evapotranspiration can result in less streamflow. However, the seasonality effect on mean annual evapotranspiration cannot be adequately represented by phase difference between rainfall and potential evapotranspiration alone (e.g., PfE) (Hickel and Zhang, 2006; Yokoo et al., 2008). In our study, ASD, M and SI are identified as three statistically significant factors affecting the Budyko parameter in 96 selected catchments across China. Noted that ASD and SI also are climatic seasonality characteristics. These different results of these two studies maybe resulted from the climate differences in different regions, and the influencing factors considered.

While the MARS model also selected interactions affecting the Budyko curves as follows: (1) CA and ASD; (2) PDSI and SI; (3) SI and Cv; (4) IA and M (seen in Fig. 7). Overall, the CA can undermine the reducing effect of ASD on the Budyko parameter. Drought and uneven distribution of annual rainfall enhance the reduction of Budyko parameter by SI. Lower M enhance the rising effect on evapotranspiration ratio by the IA. The interactions between climatic seasonality characteristics (i.e., PDSI and SI, SI and Cv) are very important and very subtle. Our simulations showed that the effects of climatic seasonality characteristics on water balance cannot be handled by means of total precipitation alone, as in many conceptual Budyko-type models. The role of climatic seasonality characteristics and their interactions on Budyko parameter have been shown to be important in determining long-term mean water balance. These results confirm previous observations and model predictions of the critical role played by the frequency of rainfall events and seasonal variability of climate (e.g., Yokoo et al., 2008; Wang and Tang, 2014).

In our study, taking all 12 factors consisting of natural and anthropogenic factors into the MARS model, 7 factors are selected in the final model, including ASD, SI, IA, M, Cv, PDSI and CA. The Budyko's n values estimated by the MARS model reproduce the calculated ones by the observation well for the selected 96 catchments (with R = 0.817, MAE = 4.09). Alternatively, we also assess the performance of MARS model in term of evapotranspiration. With estimated parameter n, the Choudhury's equation reproduced mean annual E well for the 96 catchments with R of 0.917 and MAE of 13.5 mm. Without considering the agricultural activities, 4 factors are selected in the final model, including M, ASD, SI, and PDSI. Two pairs of interactions were identified by the MARS: (1) PDSI and SI, (2) ASD and M. While this MARS model performs less well on the E calculation with R is 0.751 and MAE is 38.4 mm. Five factors (PfE, ASD, Cv, Rr and M) were selected in the final MARS model by Shao et al. (2012) using 241 Australian catchments. The performance of MARS model in term of E was assessed with R of 0.911 and MAE of 43 mm. They revealed that the interaction between ASD and Cv can reduce the value of the Budyko parameter, the interaction between ASD and Rr can also lead to a smaller Budyko parameter, while the interaction between Rr and M will lead to an increase in the Budyko parameter. MARS model can reproduce E in 241 Australian catchments better than 96 Chinese catchments since the agricultural conditions affect water balance and cannot be ignored across China.

5.2. Agricultural activities factors' effect on regional water availability assessment

With the agricultural activities, the MARS model reproduces mean annual E well for the 96 catchments with the R is 0.917 and the MAE is 13.5 mm. Without the agricultural activities, the MARS model performs the calculated E by the observation with the R is 0.751 and the MAE is 38.4 mm. It can be seen that agricultural activities have much effect on regional water availability assessment. In particular, the first interaction identified by the MARS model affecting the Budyko parameters is the cultivated land area and the average storm depth (Fig. 7(a)). Obviously, cultivation can be affected by climate change due to the ongoing

intensifications of regional hydrological cycles with the alterations of precipitation, runoff, infiltration, groundwater flow, evapotranspiration, and soil moisture in many parts of the world during past century (Alan et al., 2003; Huntiugton, 2006; Wang et al., 2017). Yokoo et al. (2008) explored the effects of seasonal variability of climatic inputs on mean annual and monthly water balances and the roles of climate, soil properties and topography in modulating these impacts, and found that the effects of seasonality are most important when the seasonal variabilities of precipitation and potential evapotranspiration are out of phase, and in arid climates. In our study, the CA was found to undermine the reducing effect of ASD on the Budyko parameter, this general conclusion confirms and extends the results of the previous work done by Yokoo et al. (2008), Shao et al. (2012) and Liang et al. (2015).

Well known that the anthropogenic factors, such as harvesting, clearing, and fertilization, have been found to change both the vegetation and the evapotranspiration capacity (Ma et al., 2008; Roderick and Farquhar, 2011; Wang and Hejazi, 2011; Li et al., 2013), further affect the regional water availability and hydrological cycle. Moreover, anthropogenic interventions tend to have increasing or enhancing influence on hydrological cycle because the increasing population, expanding cultivation, irrigation, afforestation, and enhancing deforestation (Scanlon et al., 2007; Roderick and Farquhar, 2011; Liu et al., 2017). de Vrese et al. (2016) confirmed that irrigation has a direct effect on regional atmospheric circulations and associated precipitation patterns such as the South and East Asian monsoon. Cultivation and irrigation are not only affected by changing climate conditions and altering land cover/use, but in turn have a substantial effect on them. Our findings here enhance that changes in parameter n could be captured by interaction between the vegetation and effective irrigated area in the selected 96 catchments across China, which have not been quantified assessing before.

Land cover/use, for example, vegetation cover, is also an important factor in Budyko parameter n estimation for it can directly influence rainfall redistribution, e.g., vegetation coverage controls water interception, and roots control infiltration, uptake, recharge, and runoff (Donohue et al., 2007, 2010; Gentine et al., 2012; Xu et al., 2013). Vegetation cover cannot be simply attributed to catchment characteristics, or human activities, which would overestimate the impact of local human activities on changes in Q, for that the vegetation information reflects the integrated landscape and climatic features (Donohue et al., 2007). Recent years, many studies have investigated the role of vegetation in the Budyko framework, e.g., Yang et al. (2008, 2009) indicated that the leaf area index have a high correlation with the Budyko parameter, they further parameterized the parameter using the variable NDVI, and found that it is quite difficult to generalize the vegetation impact on the parameter. Donohue et al. (2007, 2010) declared that models considering the vegetation information can improve the performance of the Budyko curve. Shao et al. (2012) estimated the Budyko parameter and observed large impact of forest coverage on Budyko parameter. Li et al. (2013) developed a simple parameterization for Budyko parameter based solely on remotely sensed vegetation information. Xu et al. (2013) indicated that the variance explained by NDVI seems low (11%), and much lower than the result from Li et al. (2013), they evolved that this phenomenon is resulted from the cross correlations of NDVI with other factors. Wang and Tang (2014) identified vegetation and rainfall are the dominant controlling factors on Budyko parameter. Based on the approximately linearized relationship between the Budyko parameter and vegetation cover, Greve et al. (2014) assessed the trend in wetting and drying over land across the globe, and Singh and Kumar (2015) quantified the vulnerability of water availability in India due to climate change. Subsequently, Liang et al. (2015) reveals that changes in Budyko parameter n could be captured by the relative area of the ecological restoration measures in the 14 catchments in China's Loess Plateau. Compared to the previous studies, our results emphasize the importance of agricultural activities (i.e., CA and IA) in regulating ecohydrologic processes. The results could provide a new idea to assess the Budyko-type equations parameters and facilitate a wider application of the Budyko framework in investigating the interactions between the climate, vegetation, hydrologic cycle, and agricultural activities.

5.3. Uncertainty of the interactions between influencing factors

In this paper, we considered 12 influencing factors for the collected 96 catchments across China. Although inclusion of more climatic factors and catchment characteristics can eliminate the problem of biased sampling and reduce model uncertainty (Shao et al., 2012), only the first order interaction (i.e., pairwise interactions) identified by MARS model were used to provide the hydrological interpretations for the model components, indeed there exists a potential error. Meanwhile, the model components can affect each other on multidimensional scale, not only the pairwise interactions existed, there are still some uncertainties in the identification analysis on the dominant interactions between climatic seasonality, catchment characteristics and anthropogenic factors for Budyko curves. In our study, four pairwise interactions were revealed by MARS model, i.e., CA and ASD, PDSI and SI, Cv and SI, IA and M. The interaction between CA and ASD shows that the cultivation can weaken the reducing effect of high ASD on the Budyko parameter estimating. However, for catchments with crops planting, this reducing effect tends to be weakened (Fig. 7(a)). In principle, this reduction should be enhanced when the CA increases. Fig. 7 shows that there are some biases in two pairwise interactions comparing with the Budyko parameter n calculated by observation for all 96 catchments. In order to clearly investigate how large the uncertainties resulted from these two interactions, Fig. 9 is plotted to show the biases of two pairwise interactions comparing to the Budyko parameter n calculated by observation for all 96 catchments. It can be seen that these large biases existed in the catchments with small Budyko parameter values, which is also verified by Fig. 7(a) and (d). Overall, the relative errors of these two interactions (i.e., ASD and CA, IA and M) comparing to the Budyko parameter n calculated by observation are 9.1% and 1.8%, respectively. These biases in the data set is a likely cause of the inconsistent relationship for the catchments with low ASD, CA, IA and M values. The identification of the partitioning process of P is difficult due to the fact that it is controlled by various controls and complex internal relations in the controls, especially in the small catchments, where the interaction between influencing factors and the hydrological cycle becomes more complex. Therefore, these uncertainties requires further study, especially focused on interactions differences spans small to large scale catchments.

Furthermore, the results and conclusions from this study are potentially useful for interpreting annual and seasonal water balances in different catchments, and comparing catchments in different parts of the world on the basis of their dominant process controls, although the current model was developed using long-term average state variables (multi-years mean) with results reflecting long-term equilibrium conditions of water partitioning in basins. Specially, deep insight into the interactions between climatic seasonality characteristics, catchment characteristics, and anthropogenic controls on long-term average water balance gained in this study can help formulate new approaches to catchment classification and similarity analyses. Further study about this topic can go a long way towards assisting with predicting the hydrological responses of ungauged basins.

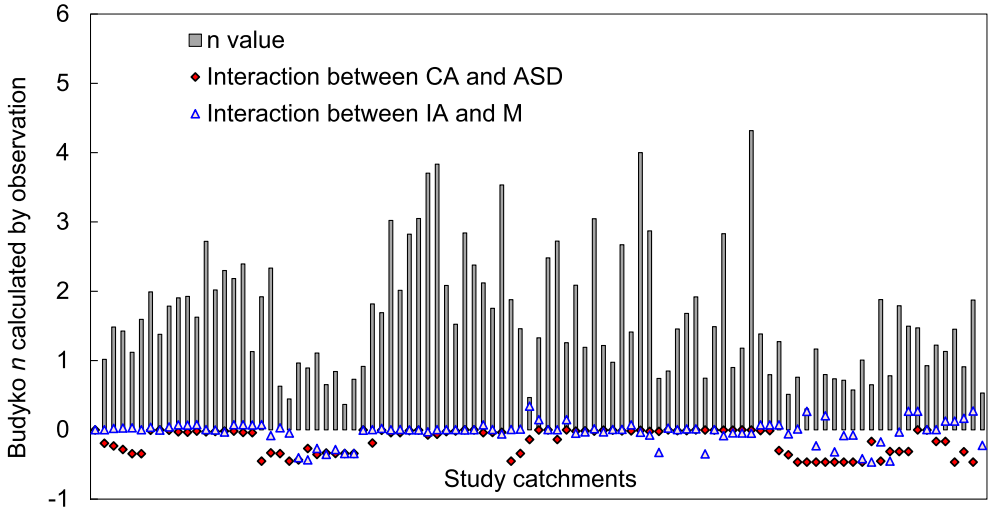

Fig. 9. Bias of two pairwise interactions (CA and ASD, IA and M) comparing to the Budyko parameter *n* calculated by observation for all 96 catchments.

6. Conclusions

In this paper, 12 influencing factors, including the catchment characteristics (M, Rr, PAWC), climatic seasonality characteristics (ASD, CI, Cv, SI, PDSI, SIM, PfE) and agricultural activities (IA, CA) were identified to be related with Budyko-type equation parameter spatially change. Correlations between climatic seasonality characteristics and catchment characteristics, agricultural activities are significant and these influencing factors are interconnected, which potentially tend to affect the Budyko-type equation parameter estimation.

A non-parametric regression technique, the multivariate adaptive regression splines (MARS) model was employed to identify the dominant interactions between climatic seasonality, catchment characteristics, and agricultural activities on Budyko-type equation parameter *n* (i.e., Budyko curve for "specific basin") estimation. The MARS model revealed that only seven factors are selected in the final model. For our collected 96 catchments across China, there are three significant factors (i.e., ASD, M and SI) affecting the Budyko parameter's estimation at different values ranges. The selected factors' interactions affecting the Budyko parameter *n*, can be summarized as follows: (1) The Budyko parameter value can be reduced when the ASD is larger than 46.78 mm, while catchments with cultivation can undermine the reducing effect of ASD. (2) The interaction of PDSI and SI is to reduce the Budyko parameter when the PDSI is less than -0.740 and the SI is higher than 0.797. (3) Budyko parameter *n* is small when the SI is less than 0.797 and the Cv is less than 0.140, or when the SI is larger than 0.797 and the Cv is higher than 0.230. (4) The interaction between the IA and M shows that the Budyko parameter *n* value is larger when the IA is lower than 4.34% and the M is lower than 34.56%, or when IA is higher than 4.34% and the M is lower than 34.56%.

Noted that agricultural activities can change both the vegetation and the evapotranspiration capacity, our study quantitatively assessed this effect and emphasized the importance of agricultural activities in regulating ecohydrologic processes. The good performance of the MARS model in the Budyko parameter estimating was gained with the correlation coefficient (R) is 0.817 and the mean absolute error (MAE) is 4.09. The uncertainties of the interactions are likely causes of the inconsistent relationship for the catchments with low ASD, CA, IA and M values, especially in the small catchments, where the interaction between influencing factors and the hydrological cycle becomes more complex.

Acknowledgments

This work was jointly supported by the National Science Foundation of China (51379057, 51779073), the Fundamental Research Funds for the Central Universities (2015B14114, 2017B21414), the National "Ten Thousand Program" Youth Talent, and the QingLan Project. Thanks to the National Meteorological Information Center, China Meteorological Administration (http://cdc.cma.gov.cn) for offering the meteorological data. Cordial thanks are extended to the Editor, Professor Geoff Syme, and two anonymous reviewers for their critical and constructive comments which highly improve the quality of the manuscript.

References

Alan, D., Justin, Z., Edwin, S.P.M., Bart, N., Eric, F.W., Dennis, P.L., 2003. Detection ofintensification in global and continental-scale hydrological cycles: temporalscale of evaluation. J. Clim. 16, 535–547. https://doi.org/10.1175/1520-0442(2003) 016<0535:DOIIGA>2.0.CO;2.

Ananthakrishnan, R., Soman, M.K., 1989. Statistical distribution of daily rainfall and its association with the coefficient of variation of rainfall series. Int. J. Climatol. 9 (5), 485–500. https://doi.org/10.1002/joc.3370090504.

Berghuijs, W.R., Woods, R.A., Hrachowitz, M., 2014. A precipitation shift from snow towards rain leads to a decrease in streamflow. Nat. Clim. Change 4 (7), 583–586. https://doi.org/10.1038/nclimate2246.

Brown, A.E., Zhang, L., McMahon, T.A., Western, A.W., Vertessy, R.A., 2005. A review of paired catchment studies for determining changes in water yield resulting from alterations in vegetation. J. Hydrol. 310, 28–61. https://doi.org/10.1016/j.jhydrol.2004.12.010.

Bonta, J.V., 2004. Development and utility of huff curves for disaggregating precipitation amounts. Appl. Engineer. Agric. 20 (5), 641–656 https://doi.org/10.13031/2013.17467.

Budyko, M.I., 1958. The Heat Balance of the Earth's Surface, translated from Russian by N.A. Stepanova. U.S. Dept. Commerce, Washington, DC.

Budyko, M.I., 1974. Climate and Life. Academic Press, p. 508.

Chen, X., Alimohammadi, N., Wang, D., 2013. Modeling interannual variability of seasonal evaporation and storage change based on the extended Budyko framework. Water Resour. Res. 49, 6067–6078. https://doi.org/10.1002/wrcr.20493.

Choudhury, B.J., 1999. Evaluation of an empirical equation for annual evaporation using field observations and results from a biophysical model. J. Hydrol. 216, 99–110. https://doi.org/10.1016/S0022-1694(9800293-5.

de Vrese, P., Hagemann, S., Claussen, M., 2016. Asian irrigation, African rain: remote impacts of irrigation. Geophys. Res. Lett. 43, 3737–3745. https://doi.org/10.1002/2016GL068146.

Dietrich, W.E., Perron, J.T., 2006. The search for a topographic signature of life. Nature 439 (7075), 411–418. https://doi.org/10.1038/nature04452.

Döll, P., Siebert, S., 2002. Global modeling of irrigation water requirements. Water Resour. Res. 38 (4), 1037 https://doi.org/1029/2001WR000355.

Donohue, R.J., Roderick, M.L., McVicar, T.R., 2007. On the importance of including vegetation dynamics in Budyko's hydrological model. Hydrol. Earth Syst. Sci. 11, 983–995. https://doi.org/10.5194/hess-11-983-2007.

Donohue, R.J., Roderick, M.L., McVicar, T.R., 2010. Can dynamic vegetation information improve the accuracy of Budyko's hydrological model? J. Hydrol. 390 (1–2), 23–34.
Donohue, R.J., Roderick, M.L., McVicar, T.R., 2012. Roots, storms and soil pores: incorporating key ecohydrological processes into Budyko's hydrological model. J. Hydrol. 436, 35–50. https://doi.org/10.1016/j.jhydrol.2012.02.033.
Fang, K., Shen, C., Fisher, J.B., Niu, J., 2016. Improving Budyko curve-based estimates of long-term water partitioning using hydrologic signatures from GRACE. Water Resour. Res. 52, 5537–5554. https://doi.org/10.1002/2016WR018748.
Friedman, J.H., 1991. Multivariate adaptive regression splines (with discussion). Ann. Stat. 19, 1–141.
Fu, B.P., 1981. On the calculation of the evaporation from land surface. Sci. Atmos. Sin. 5 (1), 23–31 (in Chinese).
Gentine, P., D'Odorico, P., Lintner, B., Sivandran, G., Salvucci, G.D., 2012. Interdependence of climate, soil, and vegetation as constrained by the Budyko curve. Geophys. Res. Lett. 39, L19404. https://doi.org/10.1029/2012GL053492.
Greve, P., Orlowsky, B., Mueller, B., Sheffield, J., Reichstein, M., Seneviratne, S.I., 2014. Global assessment of trends in wetting and drying over land. Nat. Geosci. 7 (10), 716–721. https://doi.org/10.1038/ngeo2247.
Greve, P., Gudmundsson, L., Orlowsky, B., Seneviratne, S.I., 2015. Introducing a probabilistic Budyko framework. Geophys. Res. Lett. 42, 2261–2269. https://doi.org/10.1002/2015GL063449.
Guo, S., Guo, J., Hou, Y., Xiong, L., Hong, X., 2015. Prediction of future runoff change based on Budyko hypothesis in Yangtze River basin. Adv. Water Sci. 26, 151–160 (In Chinese with English abstract).
Hickel, K., Zhang, L., 2006. Estimating the impact of rainfall seasonality on mean annual water balance using a top-down approach. J. Hydrol. 331 (3–4), 409–424. https://doi.org/10.1016/j.jhydrol.2006.05.028.
Huntiugton, T.G., 2006. Evidence for intensification of the global water cycle:review and synthesis. J. Hydrol. 319, 83–95. https://doi.org/10.1016/j.jhydrol.2005.07.003.
Istanbulluoglu, E., Wang, T., Wright, O.M., Lenters, J.D., 2012. Interpretation of hydrologic trends from a water balance perspective: the role of groundwater storage in the Budyko hypothesis. Water Resour. Res. 48, W00H16. https://doi.org/10.1029/2010WR010100.
Jiang, C., Xiong, L., Wang, D., Liu, P., Guo, S., Xu, C.Y., 2015. Separating the impacts of climate change and human activities on runoff using the Budyko-type equations with time-varying parameters. J. Hydrol. 522, 326–338.
Jin, L., Young, W., 2001. Water use in agriculture in China: importance, challenges, and implication for policy. Water Policy 3 (3), 215. https://doi.org/10.1016/S1366-7017(01)00015-0.
Li, D., Pan, M., Cong, Z., Zhang, L., Wood, E., 2013. Vegetation control on water and energy balance within the Budyko framework. Water Resour. Res. 49, 1–8. https://doi.org/10.1002/wrcr.20107.
Liang, W., Bai, D., Wang, F., Fu, B., Yan, J., Wang, S., Yang, Y., Long, D., Feng, M., 2015. Quantifying the impacts of climate change and ecological restoration on streamflow changes based on a Budyko hydrological model in China's Loess Plateau. Water Resour. Res. 51 (8), 6500–6519. https://doi.org/10.1002/2014WR016589.
Liu, J., Zhang, Q., Singh, V.P., Shi, P., 2017. Contribution of multiple climatic variables and human activities to streamflow changes across China. J. Hydrol. 545, 145–162. https://doi.org/10.1016/j.jhydrol.2016.12.016.
Ma, Z., Kang, S., Zhang, L., Tong, L., Su, X., 2008. Analysis of impacts of climate variability and human activity on streamflow for a river basin in arid region of northwest China. J. Hydrol. 352 (3–4), 239–249. https://doi.org/10.1016/j.jhydrol.2007.12.022.
Martin-Vide, J., 2004. Spatial distribution of a daily precipitation concentration index in Peninsular Spain. Int. J. Climatol. 24 (8), 959–971. https://doi.org/10.1002/joc.1030.
McKenzie, N.J., Gallant, J.C., Gregory, L.J., 2003. Estimating water storage capacities in soil at catchment scales. Tech. Rep. 03/3, Coop. Res. Cent. for Catchment Hydrol. Clayton, Vic. Australia.
Mezentsev, V.S., 1955. More on the calculation of average total evaporation. Meteorol. Gidrol. 5, 24–26.
Milly, P.C.D., 1994. Climate, soil water storage, and the average annual water balance. Water Resour. Res. 30 (7), 2143–2156. https://doi.org/10.1029/94WR00586.
Monjo, R., Martin-Vide, J., 2016. Daily precipitation concentration around the world according to several indices. Int. J. Climatol. 36 (11), 3828–3838. https://doi.org/10.1002/joc.4596.
Ol'dekop, E.M., 1911. On evaporation from the surface of river basins. Trans. Meteorol. Obs. 4, 200.
Pike, J.G., 1964. The estimation of annual runoff from meteorological data in a tropical climate. J. Hydrol. 2, 116–123. https://doi.org/10.1016/0022-1694(64)90022-8.
Porporato, A., Daly, E., Rodriguez-Iturbe, I., 2004. Soil water balance and ecosystem response to climate change. Am. Nat. 164 (5), 625–632. https://doi.org/10.1086/an.2004.164.issue-5.
Palmer, W.C., 1965. Meteorological drought. Research Paper 45, U.S. Dept. of Commerce, pp. 58.
Potter, N.J., Zhang, L., Milly, C.D., McMahon, T.A., Jakeman, A.J., 2005. Effects of rainfall seasonality and soil moisture capacity on mean annual water balance for Australian catchments. Water Resour. Res. 41, W06007. https://doi.org/10.1029/2004WR003697.
Roderick, M.L., Farquhar, G.D., 2011. A simple framework for relating variations in runoff to variations in climatic conditions and catchment properties. Water Resour. Res 47, W00G07. https://doi.org/10.1029/2010WR009826.
Scanlon, B.R., Jolly, I., Sophocleous, M., Zhang, L., 2007. Global impacts of conversions from natural to agricultural ecosystems on water resources: quantity versus quality. Water Resour. Res. 43, W034373. https://doi.org/10.1029/2006WR005486.
Schreiber, P., 1904. Ueber die Beziehungen zwischen dem Niederschlag und der Wasserfvhrung der flvsse in Mitteleuropa. Z. Meteorol. 21, 442–452.
Shao, Q., Traylen, A., Zhang, L., 2012. Nonparametric method for estimating the effects of climatic and catchment characteristics on mean annual evapotranspiration. Water Resour. Res. 48, W03517. https://doi.org/10.1029/2010WR009610.
Shuttleworth, W.J., 1993. Evaporation. In: Maidment, D.R. (Ed.), Handbook of Hydrology. McGraw-Hill, New York, pp. 4.1–4.53.
Singh, R., Kumar, R., 2015. Vulnerability of water availability in India due to climate change: A bottom-up probabilistic Budyko analysis. Geophys. Res. Lett. 42, 9799–9807. https://doi.org/10.1002/2015GL066363.
Tan, X., Gan, T.Y., 2015. Contribution of human and climate change impacts to changes in streamflow of Canada. Sci. Rep. 5, 17767. https://doi.org/10.1038/srep17767.
Teng, J., Chiew, F.H.S., Vaze, J., Marvanek, S., Kirono, D.G.C., 2012. Estimation of climate change impact on mean annual runoff across continental Australia using Budyko and Fu equations and hydrological models. J. Hydrometeorol. 13, 1094–1106. https://doi.org/10.1175/JHM-D-11-097.1.
Walsh, R.P.D., Lawler, D.M., 1981. Rainfall seasonality: description, spatial patterns and change through time. Weather 36 (7), 201–208. https://doi.org/10.1002/j.1477-8696.1981.tb05400.x.
Wang, D., Hejazi, M., 2011. Quantifying the relative contribution of the climate and direct human impacts on mean annual streamflow in the contiguous United States. Water Resour. Res. 47, W00J12. https://doi.org/10.1029/2010WR010283.
Wang, D., Tang, Y., 2014. A one-parameter Budyko model for water balance captures emergent behavior in Darwinian hydrologic models. Geophys. Res. Lett. 41, 4569–4577. https://doi.org/10.1002/2014GL060509.
Wang, W., Ding, Y., Shao, Q., Xu, J., Jiao, X., Luo, Y., Yu, Z., 2017. Bayesian multi-model projection of irrigation requirement and water use efficiency in three typical rice plantation region of China based on CMIP5. Agric. For. Meteorol. 232, 89–105. https://doi.org/10.1016/j.agrformet.2016.08.008.
Wang, W., Zou, S., Shao, Q., Xing, W., Chen, X., Jiao, X., Luo, Y., Yong, B., Yu, Z., 2016. The analytical derivation of multiple elasticities of runoff to climate change and catchment characteristics alteration. J. Hydrol. 541, 1042–1056. https://doi.org/10.1016/j.jhydrol.2016.08.014.
Williams, C.A., Reichstein, M., Buchmann, N., Baldocchi, D., Beer, C., Schwalm, C., Wohlfahrt, G., Hasler, N., Bernhofer, C., Foken, T., Papale, D., Schymanski, S., Schaefer, K., 2012. Climate and vegetation controls on the surface water balance: Synthesis of evapotranspiration measured across a global network of flux towers. Water Resour. Res. 48, W06523. https://doi.org/10.1029/2011WR011586.
Wisser, D., Steve, F., Douglas, E.M., Fekete, B.M., Vörösmarty, C.J., Schumann, A.H., 2008. Global irrigation water demand: Variability and uncertainties arising from agricultural and climate data sets. Geophys. Res. Lett. 35, L24408. https://doi.org/10.1029/2008GL035296.
Woods, R.A., 2003. The relative roles of climate, soil, vegetation and topography in determining seasonal and long-term catchment dynamics. Adv. Water Resour. 26 (3), 295–309. https://doi.org/10.1016/S0309-1708(02)00164-1.
Xiong, L., Guo, S., 2012. Appraisal of Budyko formula in calculating long-term water balance in humid watersheds of southern China. Hydrol. Process. 26 (9), 1370–1378. https://doi.org/10.1002/hyp.8273.
Xu, X., Liu, W., Scanlon, B.R., Zhang, L., Pan, M., 2013. Local and global factors controlling water-energy balances within the Budyko framework. Geophys. Res. Lett. 40, 6123–6129. https://doi.org/10.1002/2013GL058324.
Yang, D., Sun, F., Liu, Z., Cong, Z., Ni, G., Lei, Z., 2007. Analyzing spatial and temporal variability of annual water-energy balance in nonhumid regions of China using the Budyko hypothesis. Water Resour. Res. 43, W04426. https://doi.org/10.1029/2006WR005224.
Yang, D.W., Shao, P., Yeh, J.F., Yang, H., Kanae, S., Oki, T., 2009. Impact of vegetation coverage on regional water balance in the non-humid regions of China. Water Resour. Res. 45, W00A14. https://doi.org/10.1029/2008WR006948.
Yang, H., Yang, D., Lei, Z., Sun, F., 2008. New analytical derivation of the mean annual water-energy balance equation. Water Resour. Res. 44, W03410. https://doi.org/10.1029/2007WR006135.
Yokoo, Y., Sivapalan, M., Oki, T., 2008. Investigating the roles of climate seasonality and landscape characteristics on mean annual and monthly water balances. J. Hydrol. 357 (3–4), 255–269. https://doi.org/10.1016/j.jhydrol.2008.05.010.
Zhang, L., Dawes, W.R., Walker, G.R., 2001. Response of mean annual evapotranspiration to vegetation changes at catchment scale. Water Resour. Res. 37, 701–708. https://doi.org/10.1029/2000WR900325.
Zhang, L., Hickel, K., Dawes, W.R., Chiew, F.H.S., Western, A.W., Briggs, P.R., 2004. A rational function approach for estimating mean annual evapotranspiration. Water Resour. Res. 40, W02502. https://doi.org/10.1029/2003WR002710.
Zhou, G., Wei, X., Chen, X., Zhou, P., Liu, X., Xiao, Y., Sun, G., Scott, D.F., Zhou, S., Han, L., Su, Y., 2015. Global pattern for the effect of climate and land cover on water yield. Nat. Commun. 6, 5918. https://doi.org/10.1038/ncomms6918.